Oil Shale, 2024, Vol. 41, No. 1, pp. 49–70
doi: https://doi.org/10.3176/oil.2024.1.03
ISSN 0208-189X

The depositional settings of organic-rich shale in the faulted lacustrine basin: A case study of the Y1 Member of the Yingcheng Formation in the Songliao Basin

Haoxiang Lan[a], Min Guo[a]*, Meiyan Fu[a,b]*, Jon Gluyas[c], Hengwei Guo[a], Danlong Li[a], Can Ling[a], Guanghui Duan[a], Fengcun Xing[d]

[a] College of Energy, Chengdu University of Technology, Chengdu 610059, China
[b] State Key Laboratory of Oil and Gas Reservoir Geology and Exploitation, Chengdu University of Technology, Chengdu 610059, China
[c] Department of Earth Science, Durham University, Durham, DH1 3LE, UK
[d] Institute of Sedimentary Geology, Chengdu University of Technology, Chengdu 610059, China

Received 2 October 2023, accepted 19 January 2024, available online 16 February 2024

Abstract. *Volcanic activity is often associated with the development of faulted lacustrine basins. Organic-rich shale in such basins usually contains abundant volcanic material. The influence of volcanic input on organic-rich shale deposition in the basin studied has not been discussed in detail. Based on the ten shale samples from three wells, this study analyzed the depositional environment of the Yingcheng Formation shale in the Lishu Fault Depression area of the Songliao Basin by using interpretation of logging, total organic carbon analysis, gas chromatography mass spectrometry analysis, and trace element analysis. The impact of fault break to basement and volcanic materials on the organic matter enrichment was evaluated. The results show that the organic matter of Ying 1 (Y1), the First Member of the Yingcheng Formation, in the Lishu Fault Depression is characterized mainly by type I kerogen. The shale of the Y1 Member, having high total organic carbon content, is laterally continuous and could be considered as a potential target for shale oil exploration. The shale with high total organic carbon was deposited in a freshwater deep lake under an anoxic environment. There is a significant input of volcanic material, especially around the Su2 well near the Sangshutai Fault. This study has established a sedimentary model of organic-rich shale in the faulted lacustrine basin affected by volcanic activity, which has significance for the exploration of shale oil in faulted lacustrine basins.*

Keywords: *faulted lacustrine basin, organic-rich shale, Yingcheng Formation, Y1 Member, Songliao Basin.*

* Corresponding authors, guomin10@cdut.cn, fumeiyan08@cdut.cn

1. Introduction

Shale rich in organic-rich matter commonly occurs in faulted lacustrine basins and typically has a high hydrocarbon generation potential [1–3]. It is common in the geological record of China and is hence one of the key targets for oil and gas exploration and development, and consequently important for the research of conventional oil and gas source rocks and unconventional natural gas accumulations [4, 5]. China is not the only country with lacustrine petroleum source rocks, and much of the early work has been undertaken on the Tipton and Laney members of the Green River Formation in the Gosiute Basin in western USA [1, 6, 7]. To date, in China, the Shahejie Formation in the Bohai Bay Basin, the Yanchang Formation in the Ordos Basin, and the Jurassic Daanzhai Formation in the Sichuan Basin have been studied [8–12]. Some differences emerge in these studies, particularly in the main controlling factors of the accumulation of organic matter. Some researchers indicate that high productivity is the primary factor for the formation of organic-rich shale [13–16], while others believe that the key to the high organic matter content of lacustrine shale lies in organic matter preservation [17, 18]. To further explore the impact of the sedimentary environment (high productivity) and external factors potentially affecting preservation conditions, the shale of the Y1 Member is studied in this paper.

The Songliao Basin in northeastern China is a faulted lacustrine basin formed gradually after complex tectonic evolution in the Late Paleozoic–Late Mesozoic [19–21]. The Lishu Fault Depression in the basin is rich in hydrocarbons, sourced from the shale of the Y1 Member. Previous studies have evaluated the organic geochemistry of the shale and identified it as oil-prone [22, 23]. However, the controlling factors of organic matter enrichment in this lacustrine shale are still unclear. In this study, drill core samples were analyzed to understand the depositional environment and the factors that controlled organic matter enrichment, and hence identify the exploration targets in the Lishu Fault Depression.

2. Geological setting

The study area is located in the southeast uplift of the Songliao Basin. The Lishu Fault Depression is bounded by faults trending NNE-SSW and can be divided into five structural units: Central Structural Belt, Southeast Slope Belt, Northern Slope Belt, Sangshutai Sag Belt and Sujiatun Sag Belt [12, 24]. The Sangshutai Sag Belt is oriented north-south and is controlled by the Sangshutai Fault, while the other structural belts strike close to the NNE direction (Fig. 1). The formation of the Lishu Fault Depression has experienced multi-stage tectonic events, including the Late Huoshiling (K_1h), Late Yingcheng (K_1yc), Late Denglouku (K_1d) and Late Mingshui (K_2m) tectonic movements, which

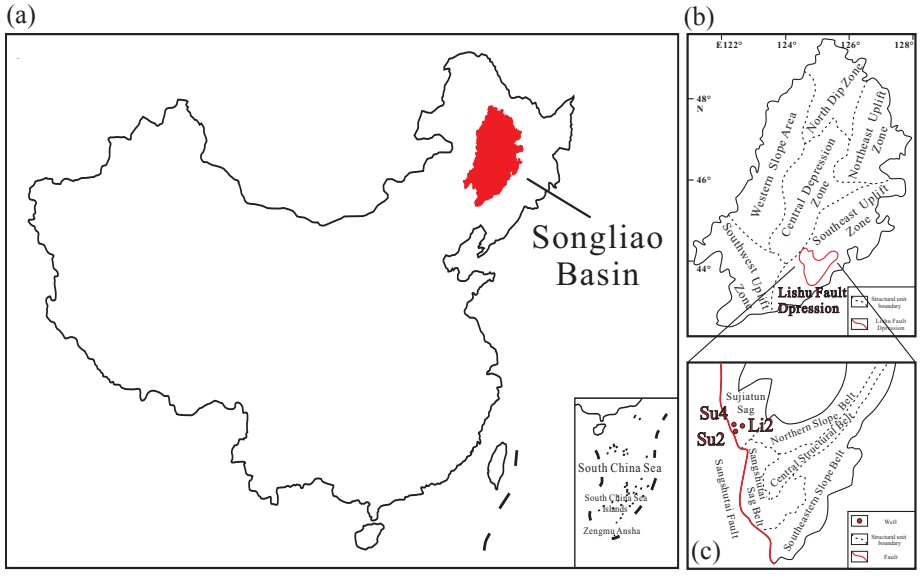

(d)

Series	Formation	Member	Lithology
Lower Cretaceous	Denglouku	D4	Red mudstone mixed with thin sandstone
		D3	Thick sandstone with thin dark/red mudstone
		D2	Thick mudstone mixed with thin sandstone
		D1	Medium–thick conglomerate
	Yingcheng	Y3	Siltstone interbedded with thin– medium fine sandstone, acid volcanic rock
		Y2	Siltstone interbedded with shale and intercalated medium fine sandstone
		Y1	Shale, intercalated with thin– medium siltstone, tuffaceous conglomerate
	Shahezi	S2	Upper gray black mudstone mixed with thin conglomerate, the lower thick conglomerate is interbedded with mudstone
		S1	Interbedded with thick sandstone and mudstone
Upper Jurassic	Huoshiling	H2	Thick–medium basic volcanic rock intercalated with conglomerate and mudstone
		H1	Dark mudstone, sandstone and sandy conglomerate

Fig. 1. Location and stratigraphy of the study area: (a) location of the Songliao Basin; (b) tectonic map of the Songliao Basin; (c) tectonic map and well location of the Lishu Fault Depression; (d) stratigraphy and lithology of the Lishu Fault Depression.

correspond to several periods of fault trap evolution, including the initial faulting period, the strong faulting period, the depression period and the inversion period, respectively. The Huoshiling tectonic time interval covered a period of intense volcanic activity in the Lishu Fault Depression and is marked by an abundance of volcaniclastic sedimentary rock in what was otherwise a shallow lake environment. In the Late Denglouku period, the depression in the study area gradually ceased, fault activity decreased, and sedimentary facies changed to braided river delta facies [12, 25–27].

The sedimentary facies of the Yingcheng Formation include the volcanic facies, fan delta, braided river delta and lacustrine facies. The lithology is

mainly represented by dark gray, grayish black mudstone and light gray siltstone with basalt, tuff and coal. The lower part of the Sujiatun Sag, where the sampling wells are located, is Upper Jurassic to Lower Cretaceous in age. The sedimentary strata from bottom to top are the Huoshiling Formation, the Shahezi Formation, the Yingcheng Formation, and the Denglouku Formation (Fig. 1). The first member of the Yingcheng Formation deposited in the fault basin can be divided into three submembers based on lithology: $Y1_1$, $Y1_2$, and $Y1_3$ (Fig. 2).

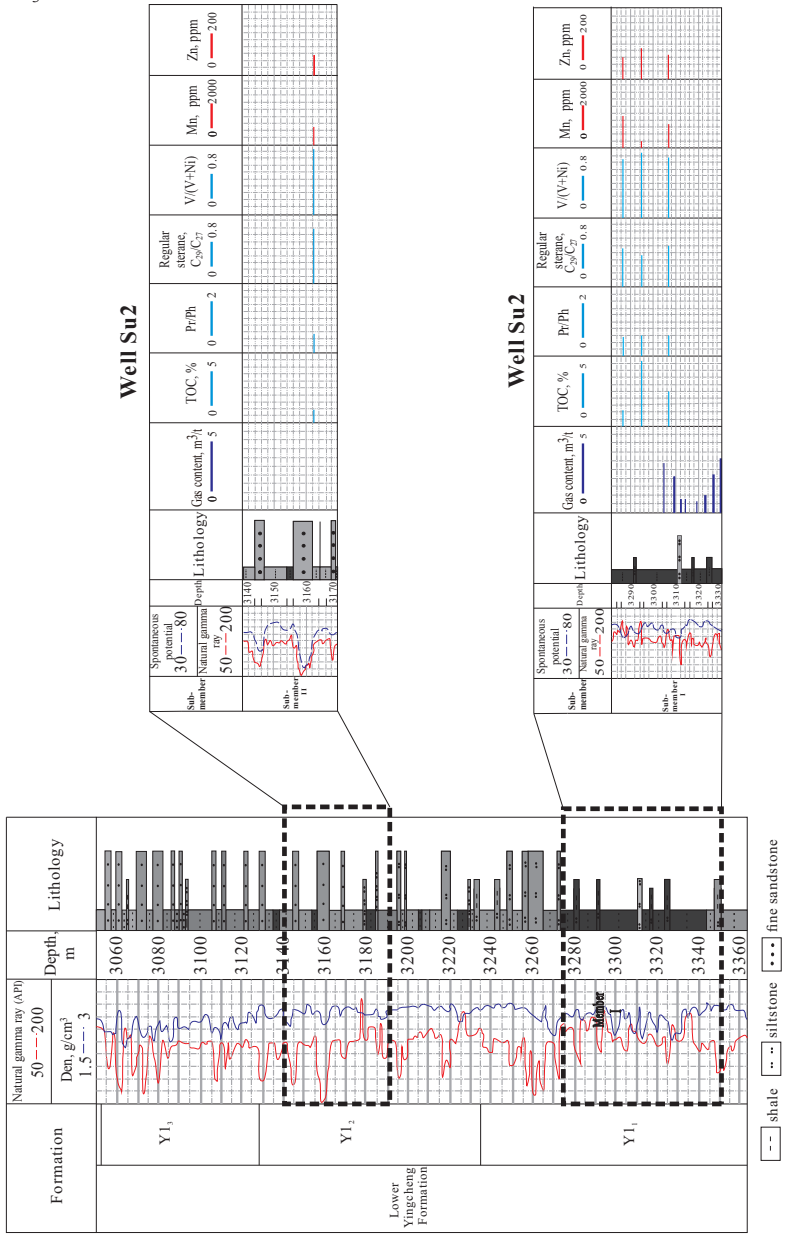

Fig. 2. Stratigraphy of the Y1 Member in Sujiatun.

3. Materials and methods

In this study, ten shale samples of the Y1 Member from three drilling wells in the Sujiatun area of the Lishu Fault Depression were selected for TOC determination, kerogen type analysis, biomarker compound determination, saturated hydrocarbon analysis, and trace element measurement.

3.1. Total organic carbon content measurement

The organic carbon content in the shale samples was analyzed according to the GB/T19145-2003 standard (China), using the CS230 carbon/sulfur analyzer (LECO, the United States). The crushed sample was first sieved with a 200-mesh sieve, then treated with hydrochloric acid solution to remove inorganic carbon from the sample, and finally dried at 50 °C for ten hours. After the above treatment, the carbon sulfur analyzer was used to measure and calculate the total organic carbon (TOC) content.

3.2. Gas chromatography analysis

The soluble organic matter was extracted from the shale, using chloroform and the Soxhlet apparatus for 72 hours. The asphaltene in the soluble organic matter was removed from the extract by precipitation with n-hexane, followed by filtration. These deasphalted extracts were fractionated on silica gel, using alumina column chromatography. The saturated hydrocarbons, aromatic hydrocarbons and non-hydrocarbons were separated by elution with n-hexane, toluene and chloroform/methanol (98:2). The saturated hydrocarbons were analyzed with the Agilent 7890A gas chromatograph (GC), equipped with an HP-5 capillary column (inner diameter 30 m × 0.25 mm, film thickness 0.25 μm). The inlet temperature was 300 °C, the flame ionization detector temperature was 320 °C, and the split ratio was 30:1. The saturated hydrocarbons were analyzed with GC. The GC column temperature was programmed from 80 °C to 310 °C at 5 °C/min, and then maintained at the final temperature for 50 minutes. Nitrogen was used as the carrier gas.

3.3. Gas chromatography mass spectrometry analysis

The biomarker compounds in the saturated hydrocarbons were analyzed with the Agilent 6890 GC/5973N MSD mass spectrometer (GC-MS), equipped with a DB5-MS capillary column (inner diameter 60 m × 0.25 mm, film thickness 0.25 μm). The GC column box was raised from 60 °C to 315 °C at 4 °C/min, and then maintained at 300 °C for 50 minutes for the GC-MS analysis of biomarkers in the saturated hydrocarbons. Helium was used as the carrier gas, and the split ratio was 20:1. Electron impact ionization was used at 70 eV, and the ion source temperature was 250 °C. The GC-MS system operated in a full scan mode from m/z 20 to m/z 750 and in a highly selective ion monitoring (SIM) mode.

3.4. Trace element analysis

The composition of elements in the shale samples was detected with the Optima 5300 V inductively coupled plasma atomic emission spectroscopy (ICP-AES; PerkinElmer) and the inductively coupled plasma mass spectrometry (ICP-MS; Finnigan MAT, Germany). The aliquots of 100 mg of ten bulk sample powders were dried at 100 °C for two hours and dissolved in mixed solutions composed of 4 mL of hydrofluoric acid, 2 mL of hydrochloric acid, 3 mL of nitric acid, 1 mL of perchloric acid and three drops of sulfuric acid. The samples dissolved in solutions were heated to about 200 °C for four hours until white smoke appeared above the residuum. Then 5 mL of chloroazotic acid were added to the solutions to extract the elements. The solutions were transferred to a 50 mL volumetric flask, diluted with deionized water to volume. After that, the major elements were tested by ICP-AES and the trace elements by ICP-MS.

4. Results

4.1. Abundance of organic matter

As shown in Table 1 and Figure 2, the organic carbon content of the first and second submembers of the Y1 Member range from 0.76% to 4.66%, with an average value of 1.79%. The burial depth of the Y1 Member in the Su2 well ranges from 3162.17 to 3306.6 m, with the TOC content of 0.86% to 4.66%. The burial depth of the Y1 Member in the Su4 well ranges from 3148.73 to 3152.23 m, and the TOC content is 0.88% to 3.89%. The burial depth of the Y1 Member in the Li2 well ranges between 2825.5 and 2908 m, and the TOC content is 0.76% to 0.84%. The content of chloroform asphalt "A" varies between 0.036% and 0.3943%, with an average value of 0.085% (Table 1). According to the evaluated standard of argillaceous source rock, the content of chloroform asphalt "A" indicates that the shale of the Y1 Member is a good source rock.

4.2. Organic matter type

The type of organic matter is an important index for the evaluation of source rocks. Generally, the kerogen hydrogen index (CIA), hydrogen index (HI), oxygen index (OI) and saturated hydrocarbon spectrogram are used to distinguish the type of organic matter [28–30]. With the thermal maturation of source rock, type I organic matter has a very high hydrogen index and a very low oxygen index, type II organic matter has a high hydrogen index and a high oxygen index, and type III organic matter has a very low hydrogen index and a very high oxygen index [30, 31]. By using the pyrolysis analysis to test the hydrogen and oxygen indices in the shale of the Y1 Member, it is found that the hydrogen index value in the shale is from 13 to 31, and the oxygen index

Table 1. Organic matter abundance indices of the Y1 Member in the study area

Well	Depth, m	TOC, %	Chloroform asphalt "A", W%	Ro, %
S2-1	3162.17	0.86	0.0360	2.14
S2-3	3286.55	1.09	0.0460	2.15
S2-4	3294.70	4.66	0.0546	2.17
S2-5	3306.60	2.46	0.0361	2.19
L2-1	2908.00	0.76	0.0719	1.92
L2-2	2825.50	0.84	0.0384	1.83
S4-1	3148.73	1.27	0.0650	1.95
S4-2	3149.53	0.88	0.0512	1.98
S4-3	3151.53	1.19	0.0565	2.10
S4-4	3152.23	3.89	0.3943	2.13

value ranges from 2 to 21 (Table 2). The hydrogen and oxygen indices cannot effectively distinguish the kerogen types in this study, probably due to high maturity. On the other hand, the GC analysis of the saturated hydrocarbons in the study area indicates that almost all samples show the characteristics of the front peak type, and the main peak carbon is n-C_{18} (Fig. 3).

Table 2. Hydrogen and oxygen indices of the Y1 Member in the study area

Well	Depth, m	HI	OI	Main peak carbon
S2-1	3282.5	31	4	C_{18}
S2-12	3287.9	19	5	C_{18}
S2-20	3292.4	18	7	C_{18}
S2-24	3294.5	24	2	C_{18}
S2-30	3297.5	13	4	C_{18}
S2-40	3303.0	15	4	C_{18}
S2-51	3308.5	18	19	C_{18}
S2-60	3314.0	21	6	C_{18}
S2-70	3318.8	15	21	C_{18}
S2-80	3324.0	21	2	C_{18}

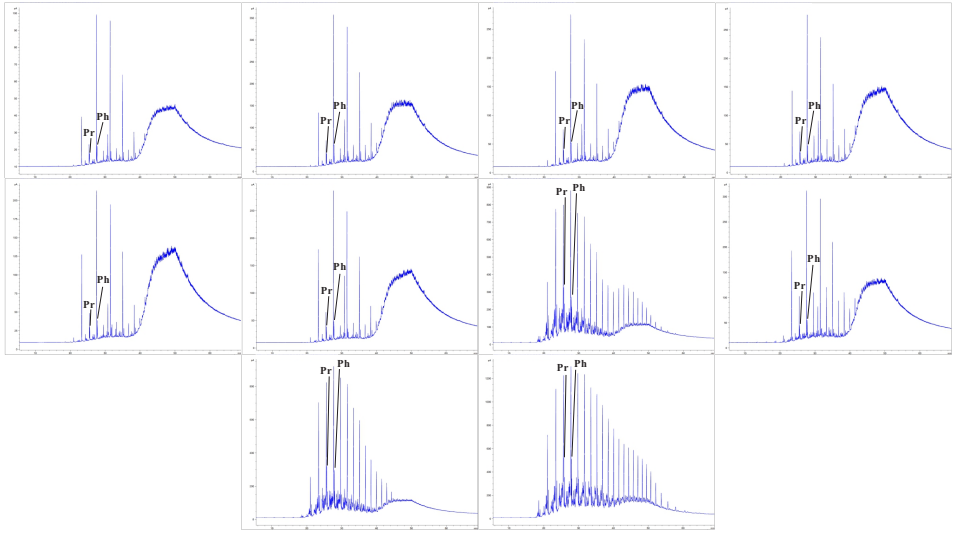

Fig. 3. Saturated hydrocarbon spectrogram of the Y1 Member in the study area.

4.3. Organic matter maturity

By measuring the vitrinite reflectance of kerogen collected from the shale of the Y1 Member in the study area, the vitrinite reflectance values are distributed between 1.83% and 2.19%, with an average value of 2.1% (Table 1). This indicates that the thermal maturity of the shale is relatively high and generally enters the high mature to overmature stage.

4.4. Composition characteristics of biomarkers

Pristane (Pr) and phytane (Ph) are two important biomarkers in the isoparaffin series. Although the Pr/Ph, Pr/C_{17} and Ph/C_{18} values are affected by biodegradation and maturity, they can generally reflect the characteristics of the shale's sedimentary environment [32, 33]. The Pr/Ph values of the ten samples from the study area range between 0.56 and 1.28, with an average value of 0.75. With the increase of organic matter maturity, the organic matter abundance of n-alkanes in the shale also increases. Pr/C_{17} decreases with the increase of the CPI value, while the value of Ph/C_{18} remains almost unchanged; the C_{29}/C_{27} values of regular steranes range from 0.37 to 0.62, with an average value of 0.5. The average value of homohopane/hopane is about 3.23 (Table 3).

4.5. Composition of trace elements

The data show a relatively high content of metals in the shale of the Y1 Member in the study area. Particularly, Mn/Fe is relatively abundant: the Mn/Fe ratios range from 55.55 to 400.27, with an average value of 187.40. The ratio of Ti/Al has almost no change in the studied samples, and the average value is about

0.06. The V/Cr ratio is 0.61–1.10, with an average value of 0.88. The Ca/Mg ratio is 0.98–3.12, on average 1.79. The Sr/Ba ratio is low, ranging from 0.8 to 1.48, with an average value of 0.98. The content of Mn ranges from 141.10 to 1505.00 μg/g, the average is 643.88 μg/g, and the content of Co is between 6.83 and 18.53, with an average of 14.02 μg/g (Table 4).

Table 3. Indices of biomarkers in the saturated hydrocarbons detected by GC analysis and sterane and terpane detected by GC-MS analysis

Well	Depth, m	Pr/Ph	Pr/C_{17}	Ph/C_{18}	CPI	Sterane C_{29}/C_{27}	Homohopane/ hopane
S2-1	3162.17	0.56	0.64	0.15	0.42	0.62	3.15
S2-3	3286.55	0.56	0.55	0.14	0.72	0.45	3.14
S2-4	3294.70	0.61	0.47	0.16	0.72	0.37	2.89
S2-5	3306.60	0.57	0.41	0.14	0.63	0.46	3.33
L2-1	2908.00	0.66	0.57	0.14	1.07	0.51	3.44
L2-2	2825.50	0.62	0.55	0.15	0.88	0.40	3.31
S4-1	3148.73	1.28	0.24	0.16	1.05	0.55	3.02
S4-2	3149.53	0.63	0.35	0.14	0.87	0.42	3.42
S4-3	3151.53	1.10	0.22	0.16	1.06	0.50	3.22
S4-4	3152.23	0.90	0.16	0.16	1.07	0.56	3.36

Table 4. Composition of trace elements in the shale of the Y1 Member

Well	Depth, m	V, μg/g	Cr, μg/g	Sr, μg/g	Mn, μg/g	Co, μg/g	V/Cr	Sr/Ba	Mn × Co
S2-1	3162.17	88.93	87.96	428.00	487.20	19.16	1.04	0.80	0.93
S2-3	3286.55	74.40	83.54	582.60	932.30	11.95	1.10	1.04	1.11
S2-4	3294.70	73.39	82.82	356.50	141.10	16.81	1.01	0.87	0.24
S2-5	3306.60	65.83	80.25	492.90	685.90	13.39	0.89	1.06	0.92
L2-1	2908.00	77.15	74.53	332.20	415.50	18.53	0.89	0.73	0.77
L2-2	2825.50	84.52	76.89	362.90	380.20	6.83	0.82	0.65	0.26
S4-1	3148.73	70.49	87.34	443.50	766.50	14.85	0.81	1.03	1.14
S4-2	3149.53	39.70	65.08	772.80	1505.00	7.16	0.61	1.48	1.08
S4-3	3151.53	75.04	97.85	416.20	769.30	15.83	0.77	0.87	1.22
S4-4	3152.23	54.34	64.83	362.20	355.80	15.67	0.84	1.27	0.56

5. Discussion

5.1. Geochemical composition of organic-rich shale of the Y1 Member

Our results show that the Y1 Member in the Lishu Fault Depression contains mainly type I and also type II kerogen. The vitrinite reflectance of shale in this area ranges from 1.83% to 2.19%, with an average of 2.1%. The maturity is relatively high, and there is a positive correlation between maturity and burial depth (Fig. 4). The degree of thermal evolution controls the content of free hydrocarbons. Ts/Tm is a thermal parameter based on the relative stability of C_{27} hopanes applicable over the range immature to mature to postmature, measured using m/z 191 [33]. It is observed that the relative abundance of Ts increases with depth, compared to Tm [34], assuming that Ts/Tm is less than 2, chloroform asphalt "A" slowly increases with the increase of TOC, and the range of chloroform asphalt "A" is 0.036% to 0.046%. When Ts/Tm is between 2 and 3, chloroform asphalt "A" increases rapidly with the increase of TOC, ranging from 0.0384% to 0.0719%. The distribution range of TOC content is 0.76% to 4.66%, the average value is 1.79%, and TOC is relatively high. The shale with higher TOC content and high maturity is found in the lower part of the Y1 Member, where the TOC values even reach about 4% (Tables 1, 3).

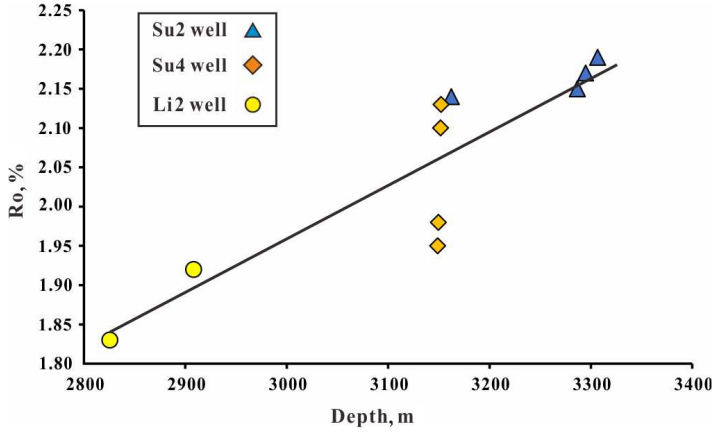

Fig. 4. Crossplot of Ro and depth of shale of the Y1 Member.

5.2. Paleoenvironmental analysis of organic-rich shale

5.2.1. Paleosalinity

There is a good linear relationship between salinity and trace element strontium. Previous studies have established Sr/Ba indicators for ancient water salinity, based on differences in the solubility of Sr and Ba elements in water with varying salinities [35, 36]. In general, a Sr/Ba ratio higher than 1.0 indicates

a marine phase, while a ratio between 1.0 and 0.5 shows a semi-saline phase, and a ratio lower than 0.5 indicates a slightly saline phase. The shale samples collected from the study area show a Sr/Ba ratio of around 1.0, implying a semi-saline environment.

5.2.2. Redox conditions

Peters et al. suggest that Pr/Ph cannot be used to indicate the redox conditions of sedimentary environment in the condition of Pr/Ph > 3.0 [33], instead of the input of terrigenous organic matter under oxidation conditions. Pr/Ph can be used to indicate anoxic sedimentary environment in the condition of Pr/Ph < 0.6. Pr/Ph < 1.0 is the cut-off value for the identification of the reduction environment. Meanwhile, because potential analytical errors cannot be eliminated in the determination of single element concentrations [37], this study uses an element ratio, such as V/Cr, to analyze the redox conditions during deposition. V/Cr > 4.25 indicates strongly reducing environments, V/Cr ratios between 2 and 4.25 show dysoxic environments, and V/Cr < 2 typically indicates oxic environments [38–40]. The Pr/Ph values of the ten samples from this study area range from 0.56 to 1.1, with an average of 0.749. Low Pr/Ph values indicate the anoxic depositional environment of the shale of the Y1 Member in the study area. V/Cr values are distributed between 0.61 to 1.10, with an average value of 0.88, indicating an oxic sedimentary environment (Table 5). As shown in Figure 5, the data are generally distributed in the area with increased oxidation degree, except for the influence of organic matter type. As individual geochemical parameters are polytropic in reflecting the paleoenvironment, synthesizing the above analyses of each parameter, the sedimentary environment of the study area is considered to be weakly oxic, i.e. weakly reductive.

Table 5. Indices of oxidation-reduction conditions of the shale of the Y1 Member

Well	Depth, m	Pr/Ph	V/Cr	Ph/C_{18}	Pr/C_{17}
S2-1	3162.17	0.56	1.04	0.15	0.15
S2-3	3286.55	0.56	1.10	0.14	0.14
S2-4	3294.70	0.61	1.01	0.16	0.16
S2-5	3306.60	0.57	0.89	0.14	0.14
L2-1	2908.00	0.66	0.89	0.14	0.57
L2-2	2825.50	0.62	0.82	0.15	0.55
S4-1	3148.73	1.28	0.81	0.16	0.16
S4-2	3149.53	0.63	0.61	0.14	0.14
S4-3	3151.53	1.10	0.77	0.16	0.16
S4-4	3152.23	0.90	0.84	0.16	0.16

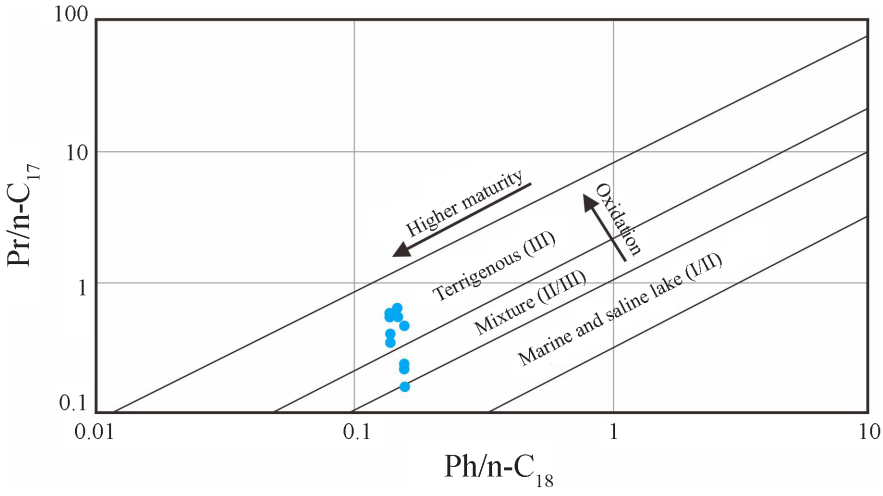

Fig. 5. Crossplot of Pr/n-C_{17} and Ph/n-C_{18} of the shale of the Y1 Member.

5.2.3. Sedimentary facies of organic-rich shale

In recent years, many researchers have pointed out that the shale of the Y1 Member is mainly deposited in semi-deep to deep lacustrine facies, and the sedimentary facies of organic-rich shale is deep lacustrine facies, mainly distributed in the Y1 Member [23, 41]. Based on the regional geological setting, lacustrine sediments developed during the sedimentary period of the Y1 Member. Thick black shale and gray black mudstone deposited in the semi-deep lacustrine and deep lacustrine subfacies can be identified in well logging.

Based on the correlation of the shale beds in the Su2 and Li2 wells (Fig. 6), it is evident that organic-rich shale mainly developed in the lower part of the Y1 Member, beds are laterally extensive, and are characterized by high organic matter abundance. There occur some sandstone interlayers in the sequence, whereas gas logging shows a high content of total hydrocarbon in the sandstone interlayers and organic matter-rich shale (TOC > 2%; Fig. 5). Compared with the first segment of the Y1 Member, the organic matter content of shale in the third segment of the Y1 and Y2 Members decreases gradually. The shale with TOC higher than 1% in the second segment of the Y1 Member is thinner, and the horizontal continuity of the shale becomes poor. The shale bed in the third segment of the Y1 Member is relatively thick and laterally extensive, but the TOC of the shale is typically lower than 1.5%.

5.3. Effect of volcanic material input

Since the Early Cretaceous, the Songliao Basin has developed into an interdivided fault basin due to the subduction of the Indian and Pacific plates beneath the Eurasian plate. In northeastern China, large-scale volcanic

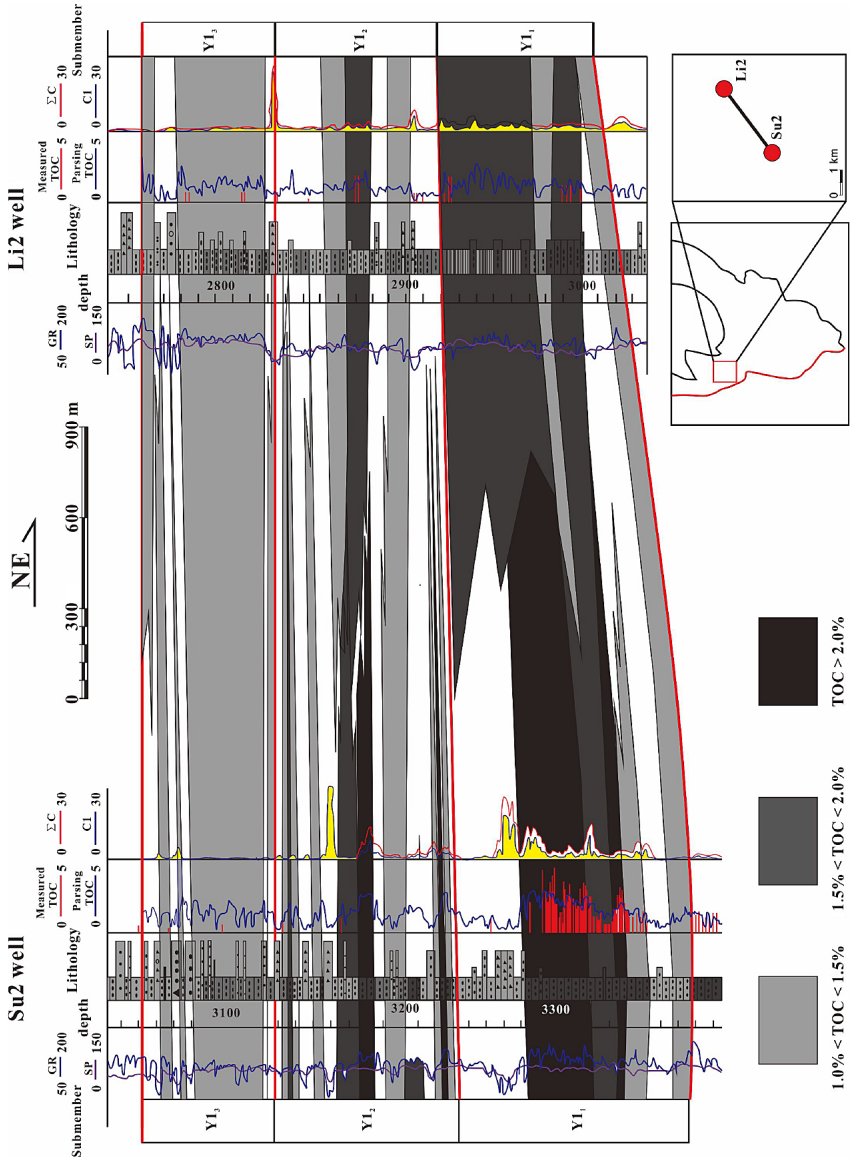

Fig. 6. Distribution of shale of the Y1 Member in the Su2 and Li2 wells.

eruptions occurred in the fault stratigraphy above the basement of the Jiameng Block. Multiple thin-bedded tuffs or tuffaceous organic-rich mud shale developed in the second member of the Shahejie Formation and the first member of the Yingcheng Formation [42–44]. A series of intermediate to acid extrusive rocks, dominated by rhyolites and other types of volcanic rocks, are found in the first and third submembers of the Y1 Member, forming a good volcanic reservoir [45, 46]. Considering the effect of volcanic material input, as indicated by the increased levels of Mn and Zn in water [47], the content of

Mn and Zn in the Su4 well in the western part of the study area is significantly higher than in the Li2 well in the eastern part of the deep lacustrine facies (Fig. 7), implying that the degree of volcanic influence varies among the wells. As shown in Figure 7, the content of Mn is negatively correlated with V/Cr, while the content of Zn also demonstrates a tendency to increase when V/Cr (oxic enrichment) decreases, implying that the reduced environment could be destroyed by volcanic material input. The two wells near the western active fault zone are greatly affected by the input of volcanic materials, and the organic matter enrichment environment is controlled by volcanism (Table 6).

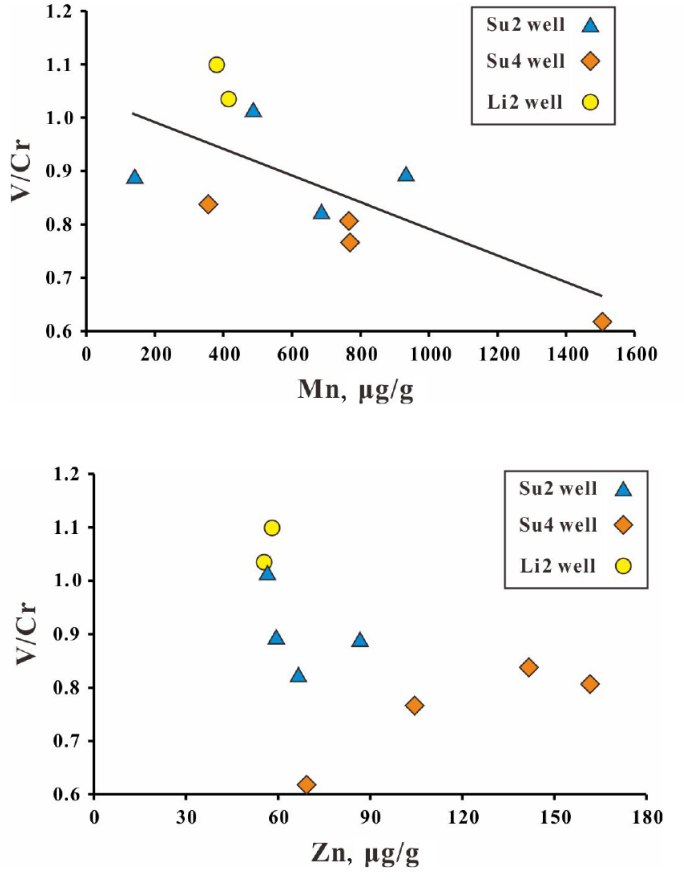

Fig. 7. Correlation diagram of Mn and Zn content and V/Cr.

Table 6. Environmental parameters of the shale of the Y1 Member

Well	Organic matter forming environment
Su2	Volcanic material input
Li2	Occlusive environment
Su4	Volcanic material input

The degree of organic matter enrichment depends on the primary productivity and preservation conditions of organic matter. The first submember of the Y1 Member in the Lishu Fault Depression had a favorable environment of high productivity and anoxic water body during the sedimentary period, which controlled the abundance, type and composition of organic matter. Organic geochemical parameters, such as the Pr/Ph ratio, can help judge the water conditions. The lacustrine facies of saline water exhibits Pr/Ph ratios from 0.2 to 0.8, demonstrating significant phytane dominance. Fresh and mildly saline water exhibits Pr/Ph ratios between 0.8 and 2.8, while Pr/Ph ratios between 2.8 and 4.0 indicate a freshwater lacustrine environment with weak reduction oxidation [48–50]. The Pr/Ph values of the organic-rich shale of the Y1 Member are relatively low, from 0.56 to 1.28, reflecting that it was formed in a saline sedimentary environment. The abundance of phytoplankton fossils is an important indicator of the trophic level, productivity and phytoplankton abundance of lacustrine basin water. The content of phytoplankton fossils in the first submember of the Y1 Member in the Lishu Fault Depression is high and the content of phytoplankton in other layers is often poor or very low, indicating that the lacustrine basin has a high level of biological productivity during the deposition of organic shale in the first submember of the Y1 Member, which is conducive to the high enrichment of organic matter.

In general, the high primary productivity and anoxic conditions of the ancient lacustrine during the development of organic-rich shale in the first submember of the Y1 Member provided conditions for the production and preservation of organic matter, thus forming a thick organic-rich shale deposit. An anoxic environment was probably caused by a stagnant deep-water environment. Characterization of water mass restrictiveness can be determined by the Mn × Co ratio. Mn × Co values $> 0.4 \times 10^{-8}$ indicate that the water body is in a stagnant environment [51]. Mn × Co ranges from 0.26×10^{-8} to 1.22×10^{-8} in the study area, with an average of 0.82×10^{-8}, indicating that the shale is deposited in a closed and stagnant environment.

Shale with low organic matter content (TOC < 1%) is mainly deposited in the environment with high terrigenous input and under oxidative conditions. Due to terrigenous input, the ratio of regular sterane C_{29}/C_{27} is high, and there is more terrigenous organic matter input. The positive correlation between sterane C_{29}/C_{27} and Pr/Ph indicates that the redox conditions changed with the changing terrigenous material input (Fig. 8).

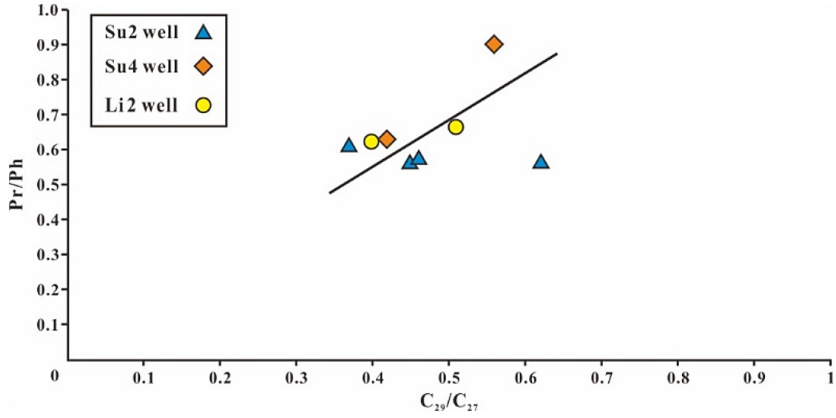

Fig. 8. Crossplot of Pr/Ph and C_{29}/C_{27} ratios.

In conclusion, the organic-rich sediments in the studied basin are deposited in a deep-water environment and have been influenced by the input of volcanic material from the eastern part of the fault. The volcanic material input is more obvious near the active fault zone in the western part of the study area, but it decreases with the increase of distance.

5.4. Sedimentary model of organic-rich shale

The formation of organic-rich shale in the studied lake basin was controlled by the input of volcanic material and paleoenvironment. The factors controlling the development of organic-rich shale are paleoproductivity and redox conditions.

The middle parts of the Y1 Member in the Su2 well and the Y1 Member in the Su4 well in the western area are rich in organic matter, due to the input of volcanic material after volcanism. The Y1 Member in the Su4 well in the west shows a relatively high content of Mn and Zn, Pr/Ph and hydrogen index. However, the Y1 Member in the Li2 well in the center of the lacustrine basin demonstrates a relatively low content of Mn and Zn and Pr/Ph, and a relatively high Mn × Co ratio, implying an anoxic and occlusive environment. Therefore, the sedimentary model of organic-rich shale in the faulted lacustrine basin, affected by volcanism, has been established (Fig. 9).

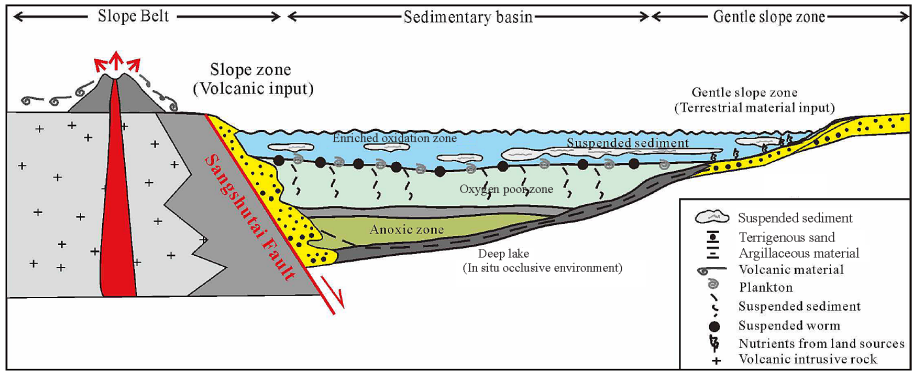

Fig. 9. Sedimentary model of organic-rich shale in the study area.

6. Conclusions

1. The shale of the Y1 Member of the Yingcheng Formation in the Lishu Fault Depression has a high abundance of organic matter and good kerogen type, mainly type I. The thermal maturity of the shale is high and generally reaches the high mature to overmature stage.
2. The shale of the $Y1_1$ submember is deposited in an oxygen-poor, stagnant and occlusive saline water environment. The shale has a high total organic carbon content and high maturity, and it is distributed in the lower part of the Y1 Member, with good horizontal continuity.
3. The organic matter enrichment environment in the study area is a closed deep-water environment and it has been affected by volcanic material input. The volcanic material input environment with organic matter enrichment has developed in the western part of the study area, near the active fault zone.

Acknowledgments

We would like to thank the SINOPEC Science and Technology Department that funded this research under the "Geological Conditions and Key Technologies of Shale Gas Enrichment in Songnan Fault Depression" project No. P17027-5. The publication costs of this article were partially covered by the Estonian Academy of Sciences.

REFERENCES

1. Horsfield, B., Curry, D. J., Bohacs, K., Littke, R., Rullkötter, J., Schenk, H. J., Radke, M., Schaefer, R. G., Carroll, A. R., Isaksen, G., Witte, E. G. Organic geochemistry of freshwater and alkaline lacustrine sediments in the Green River Formation of the Washakie Basin, Wyoming, U.S.A. *Org. Geochem.*, 1994, **22**(3–5), 415–440. https://doi.org/10.1016/0146-6380(94)90117-1
2. Dong, D. Z., Zou, C. N., Yang, H., Wang, Y. M., Li, X. J., Cheng, G. S., Wang, S. Q., Lu, Z. G., Huang, Y. B. Progress and prospects of shale gas exploration and development in China. *Acta Pet. Sin.*, 2012, **33**, 107–114. https://doi.org/10.7623/syxb2012S1013
3. Han, W. Z., Zhao, X. Z., Jin, F. M., Pu, X. G., Chen, S. Y., Mou, L. G., Zhang, W., Shi, Z. N., Wang, H. Sweet spots evaluation and exploration of lacustrine shale oil of the second member of Paleogene Kongdian Formation in Cangdong Sag, Bohai Bay Basin. *Pet. Explor. Dev.*, 2021, **48**(004), 777–786. https://doi.org/10.11698/PED.2021.04.10
4. Su, A., Chen, H. H., Feng, Y. X., Zhao, J. X., Nguyen, A. D. Multistage fracturing history in the Paleocene lacustrine shale oil reservoirs of the Subei Basin, Eastern China. *Mar. Pet. Geol.*, 2022, **144**, 105385. https://doi.org/10.1016/j.marpetgeo.2022.105835
5. Wang, X., Wang, M., Li, J. B., Shao, H. M., Deng, Z. X., Wu, Y. Thermal maturity: The controlling factor of wettability, pore structure, and oil content in the lacustrine Qingshankou shale, Songliao Basin. *J. Pet. Sci. Eng.*, 2022, **215**(PA), 110618. https://doi.org/10.1016/j.petrol.2022.110618
6. Surdam, R. C., Stanley, K. O. Effects of changes in drainage-basin boundaries on sedimentation in Eocene Lakes Gosiute and Uinta of Wyoming, Utah, and Colorado. *Geology*, 1980, **8**(3), 135–139. https://doi.org/10.1130/0091-7613(1980)8<135:EOCIDB>2.0.CO;2
7. Leggitt, V. L., Biaggi, R. E., Buchheim, H. P. Palaeoenvironments associated with caddisfly-dominated microbial-carbonate mounds from the Tipton Shale Member of the Green River Formation: Eocene Lake Gosiute. *Sedimentology*, 2007, **54**(3), 661–699. https://doi.org/10.1111/j.1365-3091.2007.00854.x
8. Lei, W. Z., Chen, D. X., Liu, Z. Y., Cheng, M. Paleoenvironment-driven organic matter accumulation in lacustrine shale mixed with shell bioclasts: A case study from the Jurassic Da'anzhai member, Sichuan Basin (China). *J. Pet. Sci. Eng.*, 2023, **220**(PA), 111178. https://doi.org/10.1016/j.petrol.2022.111178
9. Cheng, P., Xiao, X. M., Fan, Q. Z., Gao, P. Oil retention and its main controlling factors in lacustrine shales from the Dongying Sag, Bohai Bay Basin, Eastern China. *Energies*, 2022, **15**(12), 4270. https://doi.org/10.3390/en15124270
10. Ma, P. J., Dong, C. M., Lin, C. Y. Petrographic and geochemical characteristics of nodular carbonate-bearing fluorapatite in the lacustrine shale of the Shahejie Formation, Dongying Depression, Bohai Bay Basin. *Sediment. Geol.*, 2022, **439**, 106218. https://doi.org/10.1016/j.sedgeo.2022.106218
11. Pang, P., Han, H., Tan, X. C., Ren, S. M., Guo, C., Xie, L., Zheng, L. L.,

Zhu, H. H., Gao, Y., Xie, Y. H. Organic matter pores in the chang 7 lacustrine shales from the Ordos Basin and its effect on reflectance measurement. *Pet. Sci.*, 2022, **20**(1), 60–86. https://doi.org/10.1016/j.petsci.2022.08.031

12. Zhang, W., Jin, Z. J., Liu, Q. Y., Shan, X. C., Li, P., Liang, X. P. The C–S–Fe system evolution reveals organic matter preservation in lacustrine shales of Yanchang Formation, Ordos Basin, China. *Mar. Pet. Geol.*, 2022, **142**, 105734. https://doi.org/10.1016/j.marpetgeo.2022.105734
13. Liu, H. L., Zou, C. N., Qiu, Z., Pan, S. Q., Zhang, W. Z., Jing, Z. H., Hao, J. H., Yin, S., Wu, S. T., Li, S. X., Guo, Q. L. Sedimentary enrichment factors of extraordinarily high organic matter in the sub-member 3 of Member 7 of Yanchang Formation, Ordos Basin. *Acta Pet. Sin.*, 2022, **43**(11), 1520–1541.
14. Zhang, S. C., Zhang, B. M., Bian, L. Z., Jin, Z. J., Wang, D. R., Zhang, X. Y., Gao, Z. Y., Chen, J. F. Development constraints of marine source rocks in China. *Earth Sci. Front.*, 2005, **12**(03), 39–48.
15. Li, D. L., Fu, M. Y., Huang, Y., Wu, D., Xue, R. The characteristics and main controlling factors for the formation of micropores in shale from the Niutitang Formation, Wenshuicun Section, Southwest China. *Energies*, 2021, **14**(23), 7858. https://doi.org/10.3390/en14237858
16. Qiu, Z., Liu, B., Dong, D. Z., Lu, B., Yawar, Z., Chen, Z. H., Schieber, J. Silica diagenesis in the Lower Paleozoic Wufeng and Longmaxi formations in the Sichuan Basin, South China: Implications for reservoir properties and paleoproductivity. *Mar. Pet. Geol.*, 2020, **121**, 104594. https://doi.org/10.1016/j.marpetgeo.2020.104594
17. Imbus, S. W., Macko, S. A., Elmore, R. D., Engel, M. H. Stable isotope (C, S, N) and molecular studies on the Precambrian Nonesuch Shale: Evidence for differential preservation rates, depositional environment and hydrothermal influence. *Chem. Geol.*, 1992, **101**(3–4), 255–281. https://doi.org/10.1016/0009-2541(92)90007-R
18. Doner, Z., Kumral, M., Demirel, I. H., Hu, Q. H. Geochemical characteristics of the Silurian shales from the central Taurides, southern Turkey: Organic matter accumulation, preservation and depositional environment modeling. *Mar. Pet. Geol.*, 2019, **102**, 155–175. https://doi.org/10.1016/j.marpetgeo.2018.12.042
19. Deng, M. Z., Fang, C. M., Deng, P., Zhang, Y., Zhu, J. F. Origin of strike-slip thrust structure in Lishu area, southern Songliao Basin: a case study of Xiaokuan fault belt. *Acta Pet. Sin.*, 2020, **41**(09), 1089–1099. https://doi.org/10.7623/syxb202009005
20. Meng, F. C., Liu, J. Q., Cui, Y., Gao, J. L., Liu, X., Tong, Y. Mesozoic tectonic regimes transition in the Northeast China: Constriants from temporal-spatial distribution and associations of volcanic rocks. *Acta Petrol. Sin.*, 2014, **30**(12), 3569–3586.
21. Yang, X. B., Wang, H. Y., Li, Z. Y., Guan, C., Wang, X. Tectonic-sedimentary evolution of a continental rift basin: A case study of the Early Cretaceous Changling and Lishu fault depressions, southern Songliao Basin, China. *Mar. Pet. Geol.*, 2021, **128**, 105068. https://doi.org/10.1016/j.marpetgeo.2021.105068

22. Zhang, M., Li, H. B., Wang, X. Geochemical characteristics and grouping of the crude oils in the Lishu fault depression, Songliao basin, NE China. *J. Pet. Sci. Eng.*, 2013, **110**, 32–39. https://doi.org/10.1016/j.petrol.2013.08.013
23. Tang, Y., Yang, R. Z., Zhu, J. F., Yin, S., Fan, T. L., Dong, L. F., Hou, Y. C. Analysis of continental shale gas accumulation conditions in a rifted basin: A case study of Lower Cretaceous shale in the southern Songliao Basin, northeastern China. *Mar. Pet. Geol.*, 2018, **101**, 389–409. https://doi.org/10.1016/j.marpetgeo.2018.12.002
24. Wang, H. Y., Fan, T. L., Li, R. L., Hou, Y. C., Fan, X. S., Zhang, B. Search for hydrocarbon traps in syncline structures: A case study from the Lishu Depression of Songliao Basin, China. *J. Pet. Sci. Eng.*, 2017, **159**, 76–91. https://doi.org/10.1016/j.petrol.2017.09.016
25. Feng, Z. Q., Jia, C. Z., Xie, X. N., Zhang, S., Feng, Z. H., Cross, T. A. Tectonostratigraphic units and stratigraphic sequences of the nonmarine Songliao basin, northeast China. *Basin Res.*, 2010, **22**(01), 79–95. https://doi.org/10.1111/j.1365-2117.2009.00445.x
26. Ge, R. F., Zhang, Q. L., Wang, L. S., Xie, G. A., Xu, S. Y., Chen, J., Wang, X. Y. Tectonic evolution of Songliao basin and the prominent tectonic regime transition in eastern China. *Geol. Rev.*, 2010, **56**(02), 180–195. https://doi.org/10.16509/j.georeview.2010.02.005
27. Wang, R., Shi, W. Z., Xie, X. Y., Tang, D. Q., Manger, W., Busbey, A. B., Xu, L. T. Boundary fault linkage and its effect on Upper Jurassic to Lower Cretaceous sedimentation in the Gudian half-graben, Songliao Basin, northeastern China. *Mar. Pet. Geol.*, 2018, **98**, 33–49. https://doi.org/10.1016/j.marpetgeo.2018.08.007
28. Huang, D. F., Li, J. C., Zhang, D. J. Kerogen types and study on effectiveness, limitation and interrelation of their identification parameters. *Acta Sedimentol. Sin.*, 1984, **2**(03), 18–33.
29. Chen, J. P., Chen, J. J., Zhang, L. P., Zhong, N. N., Wang, Z. Y. New opinions on oil and gas generation and exploration in Jiuxi basin (I) – Basic petroleum and geological condition and oil-generating potential. *Pet. Explor. Dev.*, 2001, **28**(01), 19–22. https://doi.org/10.3321/j.issn:1000-0747.2001.01.007
30. Xiong, D. M., Ma, W. Y., Zhang, M. F., Wu, C. J., Tuo, J. C. New method for the determination of kerogen type and the hydrocarbon potential. *Nat. Gas. Geosci.*, 2014, **25**(06), 898–905.
31. Wang, J., Chen, J. F., Dou, Q. L. Evaluation of the hydrocarbon-generating potential for the possible hydrocarbon source rocks of the middle-upper Proterozoic in north Huabei area. *Pet. Geol. Exp.*, 2004, **26**, 206–211. https://doi.org/10.3969/j.issn.1001-6112.2004.02.014
32. Didyk, B. M., Simoneit, B. R. T., Brassell, S. C., Eglinton, G. Organic geochemical indicators of palaeoenvironmental conditions of sedimentation. *Nature*, 1978, **272**(5650), 216–222. https://doi.org/10.1038/272216a0
33. Peters, K. E., Walters, C. C., Moldowan, J. M. *The Biomarker Guide: Biomarkers and Isotopes in Petroleum Exploration and Earth History*. The Press Syndicate of the University of Cambridge, 2005.

34. Hong, Z. H., Li, H. X., Rullkötter, J., Mackenzie, A. S. Geochemical application of sterane and triterpane biological marker compounds in the Linyi Basin. *Org. Geochem.*, 1986, **10**(1–3), 433–439. https://doi.org/10.1016/0146-6380(86)90043-4
35. Zheng, R. C., Liu, M. Q. Study on palaeosalinity of chang-6 oil reservoir set in Ordos basin. *Oil Gas Geol.*, 1999, **20**(01), 20–25. https://doi.org/10.11743/ogg19990105
36. Wei, W., Algeo, T. J. Elemental proxies for paleosalinity analysis of ancient shales and mudrocks. *Geochim. Cosmochim. Acta*, 2020, **287**, 341–366. https://doi.org/10.1016/j.gca.2019.06.034
37. Algeo, T. J., Liu, J. S. A re-assessment of elemental proxies for paleoredox analysis. *Chem. Geol.*, 2020, **540**, 119549. https://doi.org/10.1016/j.chemgeo.2020.119549
38. Dill, H. Metallogenesis of early Paleozoic graptolite shales from the Graefenthal Horst (northern Bavaria-Federal Republic of Germany). *Econ. Geol.*, 1986, **81**(4), 889–903. https://doi.org/10.2113/gsecongeo.81.4.889
39. Dill, H., Teschner, M., Wehner, H. Petrography, inorganic and organic geochemistry of Lower Permian carbonaceous fan sequences ("Brandschiefer Series") – Federal Republic of Germany: Constraints to their paleogeography and assessment of their source rock potential. *Chem. Geol.*, 1988, **67**(3–4), 307–325. https://doi.org/10.1016/0009-2541(88)90136-2
40. Jones, B., Manning, D. A. C. Comparison of geochemical indices used for the interpretation of palaeoredox conditions in ancient mudstones. *Chem. Geol.*, 1994, **111**(1–4), 111–129. https://doi.org/10.1016/0009-2541(94)90085-X
41. Xu, Z. J., Wang, Y., Jiang, S., Fang, C., Liu, L. F., Wu, K. J., Luo, Q., Li, X., Chen, Y. Y. Impact of input, preservation and dilution on organic matter enrichment in lacustrine rift basin: A case study of lacustrine shale in Dehui Depression of Songliao Basin, NE China. *Mar. Pet. Geol.*, 2022, **135**, 105386. https://doi.org/10.1016/j.marpetgeo.2021.105386
42. Li, Y. H., Xu, X. Y., Zhang, J. F., Chen, S., Bai, J., Liu, W. B., Wang, Q. Y. Hybrid sedimentary conditions of organic-rich shales in faulted lacustrine basin during volcanic eruption episode: A case study of Shahezi Formation K_1sh Fm., Lishu Faulted Depression, South Songliao Basin. *Earth Sci.*, 2022, **47**(05), 1728–1747. https://doi.org/10.3799/dqkx.2022.015
43. Zhang, J. F., Xu, X. Y., Bai, J., Chen, S., Liu, W. B., Li, Y. H. Accumulation and exploration of continental shale gas resources of Cretaceous Shahezi Formation in Lishu fault depression, Songliao Basin, NE China. *Pet. Explor. Dev.*, 2022, **49**(3), 440–452. https://doi.org/10.11698/PED.20210755
44. Shi, X. M., Wei, Y. S., Zhu, H. Q., Wang, C. H., Huang, S. Q., Cheng, M. H. Pore structure characteristics and reservoir classification and evaluation of tight tuffaceous sandstone gas reservoir: Taking the tight tuffaceous sandstone of Yingcheng Formation in southern Songliao Basin as an example. *Nat. Gas Geosci.*, 2023, **34**(10), 1828–1841.
45. Huang, W., Shao, H. M., Zhao, H. L., Li, H. J. Characteristics of Yingcheng

Formation's volcanic reservoir in Xushen Gas Field in northern Songliao Basin. *Acta Pet. Sin.*, 2006, **27**(A1), 47–51. https://doi.org/10.3321/j.issn:0253-2697.2006.z1.009

46. Luo, J. L., Lin, T., Yang, Z. S., Liu, X. H., Zhang, J., Liu, S. Y. Lithofacies and reservoir quality control factors of volcanics in the Yingcheng Formation in the Shengping gas field in the Songliao Basin. *Oil Gas Geol.*, 2008, **29**(06), 748–757. https://doi.org/10.3321/j.issn:0253-9985.2008.06.007
47. Achterberg, E. P., Steigenberger, S., Klar, J. K., Browning, T. J., Marsay, C. M., Painter, S. C., Vieira, L. H., Baker, A. R., Hamilton, D. S., Tanhua, T., Moore, C. M. Trace element biogeochemistry in the high-latitude North Atlantic Ocean: Seasonal variations and volcanic inputs. *Global Biogeochem. Cycles*, 2021, **35**(3). https://doi.org/10.1029/2020GB006674
48. Powell, T. G., McKirdy, D. M. Relationship between ratio of pristane to phytane, crude oil composition and geological environment in Australia. *Nature Phys. Sci.*, 1973, **243**(124), 37–39. https://doi.org/10.1038/physci243037a0
49. Mei, B. W., Liu, X. J. The distribution of isoprenoid alkanes in China's crude oil and its relation with the geologic environment. *Oil Gas Geol.*, 1980, **1**(02), 99–115. https://doi.org/10.11743/ogg19800203
50. Fu, J. M., Sheng, G. Y., Xu, J. Y., Jia, R. F., Fan, S. F., Peng, P. A., Eglinton, G., Gowar, A. P. Application of biomarker compounds in assessment of paleoenvironments of Chinese terrestrial sediments. *Acta Geochim.*, 1991, **01**, 1–12. https://doi.org/10.19700/j.0379-1726.1991.01.001
51. Sweere, T., Boorn, S. van den, Dickson, A. J., Reichart, G.-J. Definition of new trace-metal proxies for the controls on organic matter enrichment in marine sediments based on Mn, Co, Mo and Cd concentrations. *Chem. Geol.*, 2016, **441**, 235–245. https://doi.org/10.1016/j.chemgeo.2016.08.028